Progress towards λ/20 extreme ultraviolet interferometry

K. A. Goldberg
Center for X-Ray Optics, Lawrence Berkeley Laboratory, Berkeley, California 94720 and Department of Physics, University of California, Berkeley, California 94720

R. Beguiristain
Center for X-Ray Optics, Lawrence Berkeley Laboratory, Berkeley, California 94720 and Department of Nuclear Engineering, University of California, Berkeley, California 94720

J. Bokor
Center for X-Ray Optics, Lawrence Berkeley Laboratory, Berkeley, California 94720 and Department of Electrical Engineering and Computer Science, University of California, Berkeley, California 94720

H. Medecki
Center for X-Ray Optics, Lawrence Berkeley Laboratory, Berkeley, California 94720

D. T. Attwood
Center for X-Ray Optics, Lawrence Berkeley Laboratory, Berkeley, California 94720 and Department of Electrical Engineering and Computer Science, University of California, Berkeley, California 94720

K. Jackson
Center for X-Ray Optics, Lawrence Berkeley Laboratory, Berkeley, California 94720

E. Tejnil
Department of Electrical Engineering and Computer Science, University of California, Berkeley, California 94720

G. E. Sommargren
Advanced Microtechnology Program, Lawrence Livermore National Laboratory, Livermore, California 94550

(Received 2 June 1995; accepted 23 August 1995)

Diffraction-limited optical imaging systems for extreme ultraviolet (EUV) lithography require wave front aberrations to be limited to a fraction of the EUV wavelength. Surface figure metrology and wave front measurement at this level of accuracy represent key challenges in the development of EUV lithography. We have constructed and operated a wave front measuring interferometer at 12–13 nm wavelength. This interferometer is being used to measure the aberrations in 0.1 numerical aperture Fresnel zone plate lenses. Factors limiting the resolution and accuracy of the interferometer were studied. Substantial progress toward λ/20 wave front measurement accuracy has been made.

I. INTRODUCTION

Diffraction-limited reflective optical systems for extreme ultraviolet (EUV) lithography have subnanometer surface figure error tolerances.[1,2] Multilayer coated optics require at-wavelength wave front measurement to characterize phase effects which cannot be measured by conventional interferometry. In addition, final testing and alignment of EUV optical systems will require at-wavelength testing to adjust and minimize cumulative errors.

We have previously reported[3,4] successful operation of an EUV point diffraction interferometer using an undulator radiation source and coherent optics beamline at the Advanced Light Source (ALS) at Lawrence Berkeley Laboratory. The point diffraction interferometer[5,6] (PDI) utilizes a common path, diffracted spherical reference wave front, reducing demands on the coherence length of the illumination, and eliminating the need for optical reference surfaces and beamsplitters. Static fringe pattern analysis applied to the interferometric data reveals wave front aberrations in the optics under test. In this article, we present wave front measurements of a Fresnel zone plate lens with 0.1 numerical aperture, operating at 13 nm wavelength.

II. EXPERIMENT DESCRIPTION

Shown schematically in Fig. 1, the PDI consists of a partially transmitting membrane, or ''mask,'' with a ''reference'' pinhole located near the focal plane of the optical system under test. The pinhole should be considerably smaller than the diffraction-limited focal spot to produce a highly spherical reference wave front. The central region of the wave front diffracted by the pinhole interferes with the transmitted wave front from the optical system under test. Displacement of the reference pinhole within the focal plane of the optical system introduces ''tilt'' fringes, facilitating analysis of the optical aberrations. Interference fringes are recorded by an EUV charge-coupled device (CCD) camera.

A pinhole mask, processed according to the prescription proposed by Sommargren and Hostetler[7] and fabricated by Spallas *et al.*[8] contains a square, 7×7 array of pinholes. Pinhole size and absorber thickness vary along perpendicular directions, allowing selection of the pinhole which produces optimum numerical aperture and fringe contrast. The pinholes form a grid with 40 μm spacing, and are adequately separated to allow individual pinhole illumination.

In its original design the mask consists of a 2000-Å-thick

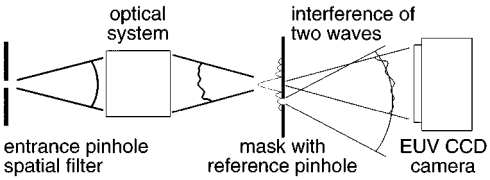

FIG. 1. A schematic description showing the key elements of the PDI (not drawn to scale). A spherical reference wave front is generated by a small pinhole in a thin, absorbing mask placed at the focus of a coherently illuminated optical system. Interference fringes are recorded by an EUV CCD camera.

Si_3N_4 membrane and a graded Co film (400–700 Å) as the absorber. The pinholes (1500–4000 Å) are patterned by electron-beam lithography and are etched completely through the Si_3N_4 membrane before the Co film deposition. This thermal evaporation process was done using care to achieve highly anisotropic deposition. This thermal evaporation process was done using care to achieve highly anisotropic deposition, which maintains the open pinholes through both the Co absorber and the Si_3N_4 membrane.

Initial PDI interferometric tests[4] revealed that to improve the reference wave front quality and fringe contrast, smaller pinholes and reduced transmission through the mask were required. Both objectives were achieved by an additional deposition step. Approximately 24 Å of chromium, followed by 240 Å of gold, were deposited by thermal evaporation without special care to achieve anisotropic deposition. This further reduced the pinhole size and also decreased transmission through the mask. The reference pinhole diameters were determined from the angle subtended by the first diffraction minima under plane-wave illumination conditions.[4] Measurements made before and after the gold deposition reveal that in nearly all cases, the apparent diameters of reference pinholes were reduced.

The mask is attached to a specially constructed $x-y$ stage with 0.01 μm motion resolution and stability, and a range of travel of several millimeters. The zone plate under test moves on a similar z-axis stage. The interferometer is mounted on an optical table to provide the stability required for the experiment. The entire system operates at a vacuum of approximately 2×10^{-6} Torr. Interferograms are recorded using an EUV CCD camera containing a Tektronix 1024 $\times$1024 pixel, back-illuminated CCD, with 25$\times$25 μm pixel size, and approximately 1 in.^{2} total area.

The light source used in these experiments is an undulator beamline operating at the ALS at Lawrence Berkeley Laboratory. The beamline incorporates a spherical grating monochromator with a resolving power of $\lambda/\Delta\lambda\approx3000$ (full width at half-maximum) at 13 nm wavelength. Beamline optics focus the beam both horizontally and vertically onto an entrance pinhole spatial filter located 2.4 m from the zone plate. The entrance pinhole diameter, which determines the spatial coherence of the zone plate illumination, was chosen as 120 μm to maximize throughput without sacrificing illumination uniformity. This diameter is small enough that the zone plate produces a diffraction-limited focal spot with a central Airy disk diameter of approximately 1700 Å in the plane of the first-order focus. Flux through the entrance pinhole is in the range of 10^{11} photons/s, depending on experimental conditions: including the wavelength, and other beamline settings. Factors limiting the resolution and accuracy of the interferometer are examined in some detail.

III. REFERENCE WAVE FRONT

The wave front emanating from the test optic interferes with the reference wave front diffracted by the reference pinhole. The optical path difference (OPD) between the two waves is measurable by the resultant interference fringes. In determining the aberrations present in the test optic, the accuracy of the interferometric measurements can thus be limited by the quality of the reference wave front. The optimum pinhole size is between 500 and 1000 Å, to properly overlap the numerical aperture of the optical system with uniform phase and sufficient flux.

The shape[4] and illumination of the reference pinhole affect the quality of the reference wave front. Since the pinhole is near the focal plane of the optic, and is displaced significantly from the optic axis (1–2 μm is typical), the pattern of illumination incident on the pinhole may not be uniform. For example, within the focal plane of an *ideal* lens with a circular pupil and 0.1 numerical aperture, at 13 nm wavelength, the Airy ring minima are separated by as little as 700 Å. The consequence of this nonuniform illumination on the reference wave front distortion is under investigation. Numerical simulations indicate that the deleterious effects of pinhole shape and illumination are reduced for smaller pinhole diameters, below 1000 Å.

IV. CHARACTERISTICS OF THE FRESNEL ZONE PLATE LENS

Zone plate lenses are critical elements in many short-wavelength applications that require concentrating or imaging elements. Zone plates were chosen as the test optics for our first interferometric measurements because of their availability at 0.1 numerical aperture, the relative simplicity of their alignment and use, and because zone plates may be used in future interferometric measurements of multilayer-coated normal-incidence reflective optical systems.

The zone plate studied in these measurements[9] was fabricated in electroplated Ni, on a Si_3N_4 membrane. The zone plate has a diameter of 200 μm, an outer zone width of 75 nm, and a focal length of 1.2 mm at 13.5 nm wavelength. This zone plate also contains an opaque central stop of 60 μm in diameter, which gives it an annular pupil.

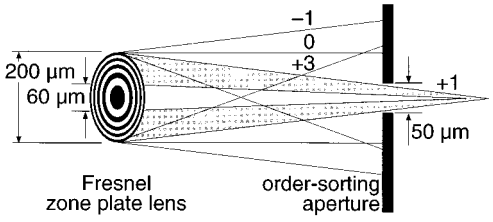

FIG. 2. Schematic of zone plate diffraction showing four of the many diffracted orders. An order-sorting aperture is used in combination with an opaque central stop to block all but the first-order focused diffraction.

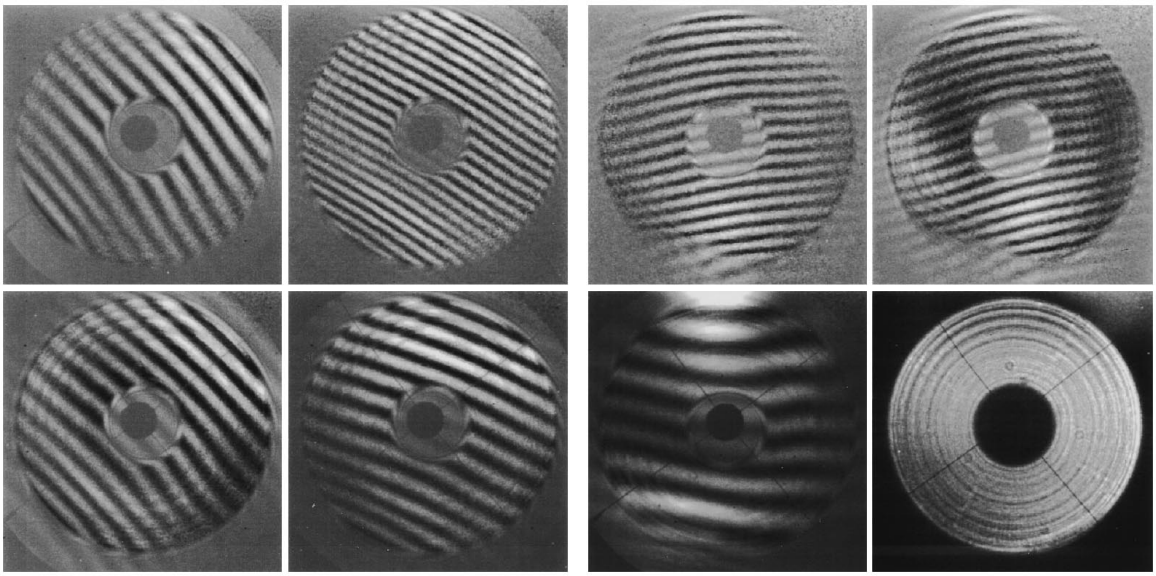

FIG. 3. Fresnel zone plate interferograms recorded at 13 nm wavelength. (a) Series 1: interferograms recorded with no upstream entrance pinhole spatial filter. (b) Series 2: recorded with a 120 μm entrance pinhole. Between each image of a series, the reference pinhole was translated laterally. The one annular image in series 2 is not an interferogram: it is an image of the first-order zone plate diffraction with no contribution from the reference wave front. To increase interferogram fringe visibility, an image like this is ''subtracted'' from the raw data in each series. The dark circle visible in the center of each image is a beamstop, held by fine wires, close to the CCD camera.

Fresnel zone plates diffract light into many separate diffraction orders, including undeviated zero-order light, higher focused orders, and divergent negative orders. A 50 μm diameter order-sorting aperture, placed approximately 1 mm from the zone plate, is used in conjunction with the 60 μm diameter opaque central stop to block light from these other orders. This configuration is shown in Fig. 2. As a further precaution to protect the CCD from zero-order radiation, a beamstop is held close to the CCD by fine wires. This is visible as a dark circle in the center of each image.

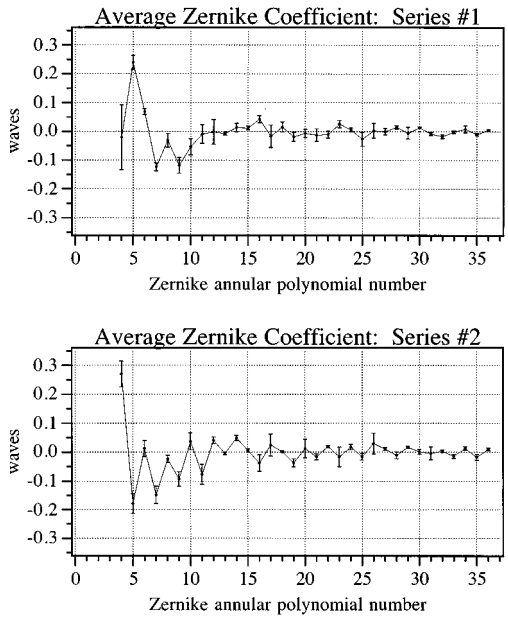

FIG. 4. Analysis of the interferometric data of series 1 and series 2. Within each series, each interferogram is analyzed separately, and then the average Zernike annular polynomial coefficients are found.

In the plane of measurement 10 cm beyond the zone plate focus, the first-order zone plate diffraction contains circular features of high spatial frequency and nonuniform distribution. We have observed similar, but unique features in 13 separate zone plates, fabricated in a similar manner.[4] Despite the presence of these features, the lower-order wave front aberrations are still easily measured.

V. ZONE PLATE WAVE FRONT MEASUREMENT

In this section we present interferometric measurements recorded during characterization and optimization studies in progress on the interferometer. Experiments have been performed using a single optical element (zone plate) under various conditions of illumination and axial rotation, and with different reference pinholes.

A. Experimental conditions

The two series of measurements presented here represent different experimental conditions. The first series of four measurements, series 1, was performed without the spatial filter entrance pinhole usually used to determine spatial coherence. This configuration of defocused and unfiltered illumination offers higher flux, yet has uncertain coherence properties. Series 2 contains three measurements, in which the zone plate was illuminated using the 120 μm diameter entrance pinhole spatial filter 2.4 m away, as indicated in Fig. 1. This configuration generates a coherent wave front for illumination of the interferometer. In addition, the zone plate was rotated axially by 139° with respect to its orientation in series 1; and a different reference pinhole was used. *Within* each series of measurements, the beamline optics and the zone plate were not adjusted; yet, for each individual measurement, the mask pinhole was translated laterally, introduc-

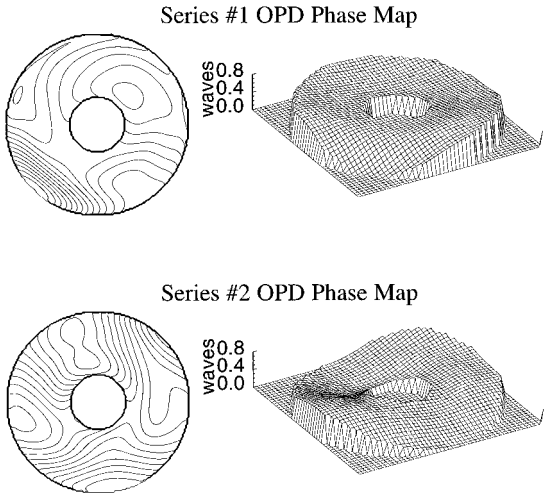

FIG. 5. The OPD phase map for each series is displayed as contour and surface plots. The contours are separated by 0.05 waves. A spike in the corner of the surface plots corresponds with the lower-right corner of the contour.

ing a change in the density and/or direction of the fringes. Interferograms from series 1 and 2 are shown in Figs. 3(a) and 3(b).

B. Analysis

The goal of the analysis is to characterize the aberrations of the zone plate lens by measuring its transmitted wave front. Interferogram analysis determines the OPD between the zone plate's wave front and the reference wave front. This measured OPD reveals the zone plate's wave front with an accuracy set by the quality of the reference wave front, and the quality of the illumination. The method of static fringe pattern analysis employed in this study is discussed in the Appendix at the conclusion of this article.

The measured OPD is described by a set of Zernike annular polynomials which are orthogonal over an annular pupil with 30% of the radius obscured.[10,11] In the normalization convention followed here, the polynomial magnitudes are bounded by $[-1, 1]$ over the annular pupil.[12] Individual measurements from within each series are combined to form an average OPD phase map. Uncertainty in the OPD measurement is determined by the variance of the aberration polynomial coefficients, and by the variance of the measured OPD at each point in the aperture.

TABLE I. Results of series 1 and series 2 interferogram analysis. All measurements are given in waves.

	Series 1	Series 2
rms wave front error	0.13	0.16
$P-V$ wave front error	0.72	0.68
Mean measurement uncertainty	0.055	0.037
Magnitudes of:		
astigmatism	0.26±0.03	0.33±0.03
coma	0.14±0.01	0.15±0.03
spherical aberration	0.03±0.02	0.02±0.01

Analyses of series 1 (no entrance pinhole) and series 2 (120 μm entrance pinhole, and rotated zone plate) data is displayed in Figs. 4 and 5, and is described numerically in Table I. "Wave front error" describes the measured aberrations, indicating deviation from a perfect spherical wave front. "Measurement uncertainty" is here defined as the standard deviation of the measured OPD at *each point* in the aperture, based on the individual OPD measurements of a series. The *mean* measurement uncertainty indicates the agreement among the individual OPD phase maps of a series. The magnitudes of the first three primary aberrations are shown in Table I. The uncertainty is determined by the variance of the data.

In both measurement series, astigmatism is the largest component of the wave front error. Two potential sources of astigmatism in the zone plate, non-normal illumination, and ellipticity, were investigated. Tilt of the zone plate axis with respect to the EUV beam axis was measured by reflecting a visible laser from the zone plate substrate. Misalignments on the order of 2 mrad were determined. In addition, the ellipticity of this zone plate has been measured[13] to be on the order of one part in 10^4. The contributions of these two effects to the zone plate astigmatism are more than one order of magnitude smaller than the observed astigmatic wave front error. The direction of the measured astigmatism in each series does not correspond with the axial rotation of the zone plate lens in series 2, with respect to series 1.

Between the two series studied here, the magnitudes of the rms and peak-to-valley wave front errors are in good agreement; yet the phase maps show clear, qualitative differences which are not attributable to the axial rotation of the zone plate. It is quite clear from these results that the illumination coherence is critical. Higher illumination coherence comes at the expense of photon flux. Further investigation is required to determine the optimum illumination conditions.

VI. CONCLUSION

We have demonstrated interferometric measurements of an EUV test wave front, with rms reproducibility of 0.06 waves. Characterization of the absolute measurement accuracy requires further work. Future improvements will accrue as we isolate systematic sources of errors due to the interferometer illumination, the reference pinhole limitations, and other imperfections in the system. Our goal is to extend this work to interferometry with reflective optical systems and $\lambda/20$ accuracy, using a beamline optimized for coherent flux.

ACKNOWLEDGMENTS

The authors gratefully acknowledge the contributions of J. P. Spallas of Livermore National Laboratory, and R. Hostetler of Ray Raskin Associates for their contributions in the fabrication of the pinhole masks. This work was supported by the ARPA Advanced Lithography Program, and by the Office of Basic Energy Science of the Department of Energy under Contract No. DE-AC03-76SF00098.

APPENDIX: FRINGE PATTERN ANALYSIS METHOD

Analysis of interferometric data reveals the OPD between the test and reference wave fronts. A wide variety of static fringe pattern analysis methods exists.[14–17] Here we employ a fringe analysis method based on the locations of the fringe minima. Comparison of multiple interferograms enables the average wave front phase surface, and measurement uncertainty to be determined.

We have implemented a software algorithm that treats the locations of the fringe minima as surfaces of constant optical path difference, separated by one wavelength. Minima are found along a direction perpendicular to the fringes, and a typical interferogram with 8–21 fringes across a 256×256 pixel image will contain 1200–3000 data points for the wave front surface fitting. The data are fit to an intermediate basis of polynomials orthogonal over the discreet domain.[18,19] The coefficients of the first 37 Zernike annular polynomials, (with 30% radial obscuration) are then calculated by a simple basis transformation. OPD tilt and defocus, which are determined by lateral and longitudinal displacements of the reference pinhole, have no physical significance for the optical aberrations being studied.[6] In addition to tilt and defocus, piston, an arbitrary overall phase offset, is not included in the analysis and comparison of multiple interferograms.

[1]M. D. Himel, in *OSA Proceedings on Soft X-Ray Projection Lithography*, edited by A. M. Hawryluk and R. H. Stulen (Optical Society of America, Washington, DC, 1993), Vol. 18, p. 1089.
[2]D. Attwood, G. Sommargren, R. Beguiristain, K. Nguyen, J. Bokor, N. Ceglio, K. Jackson, M. Koike, and J. Underwood, Appl. Opt. **32**, 7022 (1993).
[3]K. A. Goldberg *et al.*, in *Extreme Ultraviolet Lithography*, edited by D. T. Attwood and F. Zernike (Optical Society of America, Washington, DC, 1994), pp. 134–141.
[4]K. A. Goldberg *et al.*, Proc. SPIE (to be published).
[5]W. P. Linnik, Proc. Acad. Sci. USSR **1**, 208 (1933).
[6]R. N. Smartt and W. H. Steel, Jpn. J. Appl. Phys. **14**, 351 (1975).
[7]G. E. Sommargren and R. Hostetler, in Ref. 1, pp. 100–104.
[8]J. P. Spallas, R. Hostetler, and G. E. Sommargren (unpublished).
[9]E. H. Anderson *et al.*, J. Vac. Sci. Technol. B **9**, 3606 (1991).
[10]V. N. Mahajan, Opt. Photon. News **5**, 11 (1994).
[11]V. N. Mahajan, J. Opt. Soc. Am. A **3**, 470 (1986).
[12]*Optical Shop Testing*, edited by D. Malacara (Wiley, New York, 1992), Chap. 13.
[13]E. H. Anderson (private communication).
[14]*Interferogram Analysis: Digital Fringe Pattern Measurement Techniques*, edited by D. W. Robinson and G. T. Reid (IOP, Bristol, 1993), Chaps. 3 and 5.
[15]D. A. Zweig and R. E. Hufnagel, Proc. SPIE **1333**, 295 (1990).
[16]M. Takeda *et al.*, J. Opt. Soc. Am. **72**, 156 (1982).
[17]A. Choudry, Proc. SPIE **816**, 49 (1987).
[18]J. Y. Wang and D. E. Silva, Appl. Opt. **19**, 1510 (1980).
[19]D. J. Fischer *et al.*, Appl. Opt. **32**, 4738 (1993).